

CONFORMATIONS OF PROLYL-PEPTIDE BONDS IN THE BRADYKININ 1-5 FRAGMENT IN SOLUTION AND IN THE GAS PHASE

Liudmila Voronina¹, Antoine Masson^{1,2}, Michael Kamrath¹,
Franziska Schubert³, David Clemmer⁴, Carsten Baldauf^{3*} and Thomas Rizzo^{1*}

¹Laboratoire de Chimie Physique Moléculaire, École Polytechnique Fédérale de Lausanne,
EPFL SB ISIC LCPM, Station 6, CH-1015 Lausanne, Switzerland

²Present address: Lawrence Berkeley National Laboratory, Earth Sciences Division, 1 Cyclotron Rd.,
MS74R316C, Berkeley, California 94720, USA.

³Fritz-Haber-Institut der Max-Planck-Gesellschaft, D-14195 Berlin, Germany

⁴Department of Chemistry, Indiana University, Bloomington, IN 47405, United States

*To whom the correspondence should be addressed: baldauf@fhi-berlin.mpg.de, Thomas.Rizzo@epfl.ch

Abstract

The dynamic nature of intrinsically disordered peptides makes them a challenge to characterize by solution-phase techniques. In order to gain insight into the relation between the disordered state and the environment, we explore the conformational space of the N-terminal 1-5 fragment of bradykinin (BK[1-5]²⁺) in the gas phase by combining drift tube ion mobility, cold-ion spectroscopy, and first principles simulations. The ion-mobility distribution of BK[1-5]²⁺ consists of two well-separated peaks. We demonstrate that the conformations within the peak with larger cross-section are kinetically trapped, while the more compact peak contains low-energy structures. This is a result of *cis-trans* isomerization of the two prolyl-peptide bonds in BK[1-5]²⁺. Density-functional theory calculations reveal that the compact structures have two very different geometries with *cis-trans* and *trans-cis* backbone conformations. Using the experimental CCSs to guide the conformational search, we find that the kinetically trapped species have a *trans-trans* configuration. This is consistent with NMR measurements performed in a solution, which show that 82% of the molecules adopt a *trans-trans* configuration and behave as a random coil.

1 Introduction

Information about the structure and dynamics of proteins and peptides is crucial for understanding their physiological function and hence essential for diagnostics and drug design.^{1,2} X-ray crystallography and NMR spectroscopy can often successfully determine the structure of

1
2 biomolecules when they adopt well-defined secondary structures.³ However, in the case of
3 intrinsically disordered peptides, NMR spectra often represent an average over an ensemble of
4 different conformations. Moreover, crystallization for X-ray measurements is often not possible due
5 to the highly dynamic character of the disordered states.⁴⁻⁶ Many questions thus remain open
6 regarding the nature of intrinsically disordered peptides: Does their flexibility come from solution
7 conditions? What are the main factors contributing to the rapid structural changes? How many
8 well-defined conformers are converting among each other? How does recognition by receptors or
9 membrane insertion happen from a structural perspective?^{1,7,8}

10
11
12
13
14
15
16 One of the most well-studied representatives of partially disordered peptides is the nonapeptide
17 bradykinin (BK), which plays a regulatory role in the cardiovascular and nervous systems and is a
18 key reporter molecule in inflammation and pain.⁹ It was shown that in pure aqueous solution the
19 entire peptide exhibits many conformational states rather than a single, well-defined secondary
20 structure.¹⁰ In an aprotic solvent or upon interaction with lipid vesicles, however, residues 6-9 of the
21 C-terminus of BK adopt β -turn-like structures, while residues 1-5 remain 'disordered'.^{11,12} A
22 similar observation was made by Glaubitz and co-workers for BK bound to the human G-protein
23 coupled receptor B2, which was investigated by solid-state NMR: residues 6 to 8 (Ser-Pro-Phe)
24 appear ordered while residues 1 to 5 exhibit a high structural flexibility.¹³

25
26
27
28
29
30
31
32 One potential source of conformational heterogeneity of BK, as well as of many other peptides,
33 is proline *cis-trans* isomerization¹⁴, as the BK sequence contains proline in positions 2, 3 and 7.
34 However, most studies performed by NMR find that in the major conformer of BK all prolyl-peptide
35 bonds are in the *trans* conformation, both in free peptide and when bound to a receptor.^{11-13,15-18} In
36 general, *cis-trans* isomerization of the X-Pro bond is an important biological process; peptidyl-
37 prolyl *cis-trans* isomerases (PPIs), which catalyze conversion between *cis* and *trans* conformations
38 in peptides and proteins, are known to play key roles in the functioning of living cells.^{19,20} Of the
39 three known families of PPIs, a member of the cyclophilin family, PPIA, can be found in the
40 extracellular medium, where BK is acting, and is linked to, for example, inflammation scenarios^{21,22}.
41 Studies of the substrate specificity of PPIA shows activity even for the Pro-Pro prolyl-peptide bond,
42 but it is not known if BK is a substrate for PPIA in a particular physiological process.²³ Besides
43 this, the *cis-trans* states of prolyl-peptide bonds can be influenced by interactions with cations^{24,25} or
44 by stretching forces along the peptide backbone, which are induced electrostatically²⁶ or
45 mechanically.²⁷⁻²⁹

46
47
48
49
50
51
52
53
54
55
56
57
58
59
60
A powerful way to obtain insight into the nature of intrinsically disordered peptides is to study
them in the gas phase in the absence of solvent.³⁰⁻³⁹ For instance, using ion mobility spectrometry

1
2 (IMS), Bowers and co-workers investigated BK in its singly protonated and sodiated forms. They
3 observed only one peak, invariant of the charge carrier or the temperature.⁴⁰ Clemmer's group has
4 shown that the collisional cross-section (CCS) distribution of triply protonated BK produced *via* ESI
5 demonstrates the presence of at least three major conformational families,⁴¹ which were attributed to
6 different *cis-trans* isomerization states of the prolyl-peptide bonds.⁴² Although much insight can be
7 gained from IMS data, an unambiguous assignment of conformers is not possible. Ion mobility
8 provides only an average CCS that is not unambiguous for a conformational family in the gas
9 phase.⁴³ Instead, a single IMS peak may contain several distinct conformational families with the
10 same CCS.
11

12
13 The expected distribution of structures produced by electrospray is a mixture of low-energy gas-
14 phase conformers and higher energy structures that are kinetically trapped, with barriers on the
15 potential-energy surface (PES) that prevent isomerization.⁴⁴⁻⁵¹ These latter structures are
16 particularly important, as they retain information on the conformation of the molecule in solution.
17 In case of proline *cis-trans* isomerization, the energy barrier can be high enough (20-50 kJ/mol)⁴⁶ to
18 expect solution-phase isomers to be preserved as metastable, kinetically trapped species. Detailed
19 understanding of these kinetically trapped conformations would allow one to connect information
20 obtained from solution-phase and gas-phase techniques. The low-energy gas-phase conformers on
21 the other hand, may exemplify possible structure alternation upon change of environmental
22 condition as, for example, during membrane insertion. Vacuum can be understood as an extreme
23 case of an aprotic non-polar solvent lacking intermolecular interactions. Membranes are generally
24 seen as structure-inducing media, and a question was recently raised if molecular disorder is
25 possible there.⁵² Detailed conformational studies in the gas phase might shed light on this question.
26

27
28 In this work we focus on the 1-5 fragment of BK (Fig. 1), which is metabolically stable⁵³ and
29 was shown to inhibit the enzymatic activity of thrombin.⁵⁴⁻⁵⁶ Russell and co-workers⁵⁷ have
30 investigated the 1+ charge state of this molecule by IMS and H/D exchange after matrix-assisted
31 laser desorption ionization (MALDI). Three distinct structural forms were found, exhibiting a
32 relative abundance dependent on the composition of the electrospray solvent. The extended form
33 was observed when a high water concentration was used.
34

35
36 We investigate the conformational preferences of BK[1-5] in the +2 charge state by combining
37 drift tube ion mobility with cryogenic-ion spectroscopy and quantum-chemical calculations.
38 Experimental constraints are used to guide the first principles structure search and allow us to
39 identify not only the thermodynamically stable low-energy conformers, but also those that are
40 kinetically trapped. We show that *cis-trans* isomerization of BK[1-5] indeed plays a key role in
41
42
43
44
45
46
47
48
49
50
51
52
53
54
55
56
57
58
59
60

forming distinct conformational families. We identify the kinetically trapped structures and show that they have a direct relationship to those observed by NMR in solution.

2 Experimental and computational approach

Bradykinin[1-5] (RPPGF, Trifluoroacetate salt, Bachem) was purchased and used without further purification. Peptide solutions were prepared in a 49:49:2 mixture of water:methanol:acetic acid with a peptide concentration of 50 μM . In the 2+ protonation state, the extra protons are believed to reside on the arginine side chain and on the N-terminal amine.

The experimental part of this work is performed using two home-built, cold-ion spectrometers, both of which are described in detail elsewhere.^{58,59} We briefly highlight their salient features below.

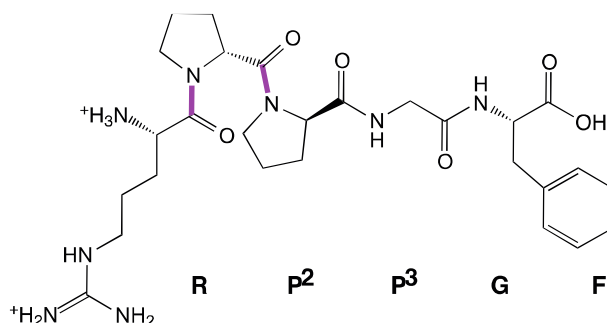


Figure 1. Chemical structure of doubly protonated bradykinin residues 1 to 5 (BK[1-5]²⁺). The two positive charges are located at the side chain of the arginine residue and at the N-terminus. The bonds around which the *cis-trans* isomerization can occur are highlighted.

2.1 Ion mobility spectrometry coupled with cryogenic ion spectroscopy

We have constructed an instrument (referred to as the IMS-CIS instrument) that combines a linear IMS drift tube with a cold ion trap and a time-of-flight mass spectrometer for measuring collisional cross-section distributions of a molecule of interest and vibrational spectra of mobility-selected ions.⁵⁹ Ions are generated by electrospray and separated according to their collisional cross-section in a 2m long drift tube, developed in the group of Clemmer⁶⁰ and incorporated into this instrument without modification. Stand-alone collisional cross-section distributions are measured at the end of the drift tube using a channeltron detector. The drift tube can be operated in two modes: as a single 2m long drift tube or as a tandem IMS-IMS instrument. In the latter mode, we pre-select a conformational family of interest in the first half of the drift tube with an ion gate, collisionally activate it in a controlled way, and observe its drift using the second half of the drift tube. Any changes in conformation upon activation manifest themselves in the latter drift-time distribution.

1
2 To perform spectroscopic studies of mobility-selected peptide ions, the ion gate at the end of the
3 drift tube is opened for 80 μ s so that only those within a pre-defined range of collisional cross-
4 sections pass through and continue to a planar ion trap where they are cooled down to \sim 10 K by
5 collisions with hydrogen. Here the ions are tagged with H₂ reporter molecules and interrogated with
6 an infrared laser. Absorption of an infrared photon leads to evaporation of hydrogen and decreases
7 the number of tagged species. The spectrum can thus be recorded by monitoring the number of
8 tagged molecules in the time-of-flight MS as a function of the laser wavelength.⁶¹
9
10
11
12
13
14
15

16 2.2 Conformer-selective cold ion spectroscopy

17 Using a separate instrument⁵⁸ (referred to as the CIS instrument) we have the ability to
18 separate conformers using IR-UV double-resonance⁶² in a cryogenic octopole ion trap and thus
19 obtain vibrational spectra for each of them. The ions are produced by a nanospray source, and after
20 passing through a metal capillary they are injected into an ion funnel. Some collisional activation of
21 the ions invariably occurs at the end of the funnel where the diameter of the electrodes is smallest.⁶³
22 After being extracted from the funnel, the ions are pre-stored in a room-temperature hexapole ion
23 trap for 70 ms, mass-selected by a quadrupole mass-filter, and then guided into a cold (4 K) octopole
24 ion trap, where they are cooled by collisions with helium. A UV laser pulse promotes the trapped
25 ions to the first electronically excited state, and since the excitation energy is above the dissociation
26 threshold, some of the parent ions fragment. All the ions are then ejected from the trap, mass-
27 selected by a second quadrupole filter, and detected by a channeltron. Detecting the number of
28 fragment ions as a function of the laser wavelength gives an electronic photofragment spectrum of
29 the parent molecule. The most abundant UV laser-induced fragment results from the loss of the
30 phenylalanine side chain (i.e., via C _{α} – C _{β} bond breakage), and we use this fragmentation channel
31 for all measurements. To obtain conformer-selective IR spectra of the cold ions, we tune the UV
32 laser wavelength to a specific transition in the electronic spectrum and introduce an IR pulse from a
33 tunable OPO 200 ns before the UV pulse. This results in depletion of the photofragment signal,
34 which is recorded as a function of IR wavelength.
35
36
37
38
39
40
41
42
43
44
45
46
47
48
49
50

51 2.3 Computational methodology

52 We generate an initial pool of calculated structures using basin-hopping, as implemented in the
53 Tinker package⁶⁴ with the OPLS-AA force field.¹⁶ The energy cutoff was set to 50 kcal/mol, and
54 the number of torsional modes was set to 20. Increasing either of these parameters does not lead to
55 a substantial increase in the number of unique structures generated. The initial pool of structures
56
57
58
59
60

1
2 was then subjected to a conformational clustering procedure from the GROMACS program
3 package,^{65,66} and only the lowest-energy representative of each cluster (cut-off 0.75 Å) were kept.

4
5 Collisional cross-sections (CCSs) first were calculated using the projection approximation (PA)
6 method⁶⁷ implemented in Sigma.⁶⁸ Knowing that this method underestimates the collisional cross-
7 sections, we selected randomly a set of 20 structures, computed their CCS with the trajectory
8 method (TM⁶⁹ in MOBCAL⁷⁰), and used linear regression to find a correspondence between CCSs
9 computed by PA and TM for our system (the coefficient calculated is 1.026). In later stages we
10 calculated the CCSs using the TM method with partial charges extracted from DFT calculations.

11
12 All DFT simulations in this work were performed in the all-electron program package FHI-aims
13 based on numeric atom-centered orbital basis sets.⁷¹ Initially the PBE functional⁷² with many-body
14 dispersion correction (MBD)^{73,74} was used. The initial relaxations were performed with the “light”
15 species defaults, while for refinement a more accurate “tight” basis was employed. For further
16 improvement of the description of the system we used the PBE0 functional.⁷⁵ These functionals,
17 and the order of increasing accuracy, were proven successful in previous studies.^{39,76-78}

18
19 For calculations of vibrational spectra we used scaling factors of 0.948 for PBE0 and 0.978 for
20 PBE. Free energies were estimated based on vibrational frequencies calculated with the PBE
21 functional at 0 K, 10 K and 300 K using harmonic oscillator and rigid rotor approximations.

2.4 Nuclear Magnetic Resonance

22
23 The NMR spectra are acquired at room temperature on a Bruker Avance III HD instrument
24 operating at 600 MHz for ¹H. We acquire TOCSY, COSY and ROESY (with the mixing time 400
25 ms) 2D ¹H NMR spectra in DMSO and use them to assist interpretation of analogous data obtained
26 in a H₂O:CD₃OH 50:50 mixture, where water suppression is performed with the presaturation
27 sequence. The relative abundances of the conformers are measured by integrating the peak volumes
28 using Mestrelab MNova NMR software.⁷⁹

3 Results

29
30 We achieve conformer selectivity in our experiments in two ways: (i) by using ion-mobility to
31 separate molecules with different cross sections by their drift time and then recording vibrational
32 spectra of the mobility-selected ions; and (ii) by performing IR-UV double-resonance spectroscopy
33 to obtain vibrational spectra of individual conformers within a mixture.

3.1 Vibrational spectra of mobility-selected ions

The ion-mobility drift-time distribution of BK[1-5]²⁺ has two well separated peaks, as shown in Fig. 2. The first peak has an unresolved shoulder and can be represented as a sum of two Gaussians, one centered at 167 Å² and the other at 170 Å². The second peak is centered at 178 Å², and its width suggests that it may also consist of more than one conformer.

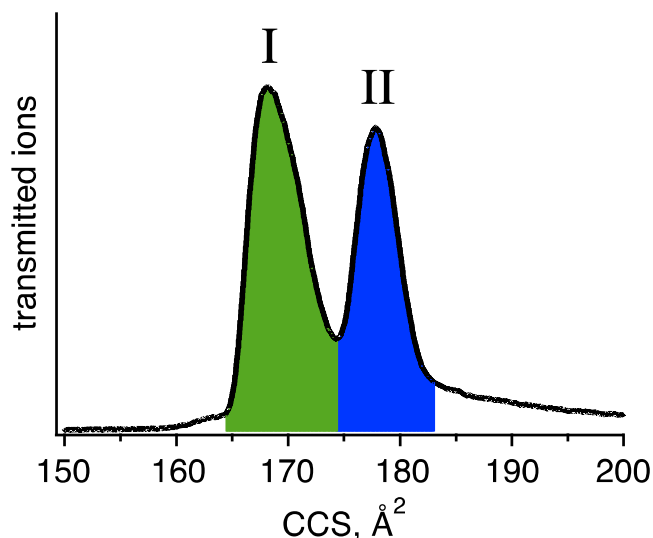


Figure 2. Collisional cross-section distribution of BK[1-5]²⁺. The extended conformers (peak II) are kinetically trapped and interconvert to more compact, stable, gas-phase structures (peak I) upon collisional activation.

When we select either of the two peaks after they drift through the first part of the drift tube and collisionally activated them, the same arrival-time distribution is produced for both peaks as they drift through the second segment of the drift tube. As shown in Fig. 3, this “annealed” distribution consists mainly of peak I with a shoulder around 176 Å², slightly more compact than the original extended conformations. We conclude that the structures contained within peak II are kinetically trapped, while peak I represents stable gas-phase structures. This type of behavior has been demonstrated previously for the full bradykinin in the 3+ charge state (BK³⁺).^{80,81}

While ion-mobility spectrometry provides a spatially averaged CCS of a molecule that reflects its overall shape, vibrational spectroscopy produces a distinct fingerprint that reflects the molecule’s precise structure. We thus select both peaks in the ion-mobility distribution and obtained their IR spectra *via* H₂-tagging spectroscopy (Fig. 4). We also obtain their vibrational spectra after annealing *via* collisional activation (50 V), and we observe that they are practically identical and contain the same bands as the vibrational spectrum of the compact structures (see SI-Fig. 2). This confirms that after collisional activation we reach the same quasi-equilibrium gas-phase distribution

independent of the starting conformation. This distribution consists of the same conformers as those under the more compact peak in the ion mobility drift-time distribution.

To assign the peaks in the IR spectra to specific vibrational modes, we had two isotopically labeled peptides synthesized by replacing the amide nitrogen of phenylalanine and glycine with ^{15}N . This substitution typically shifts the labeled NH band by $\sim 8\text{ cm}^{-1}$ to the red and allows us to identify the bands that correspond to phenylalanine and glycine NH stretches, which are labeled on Fig. 4.

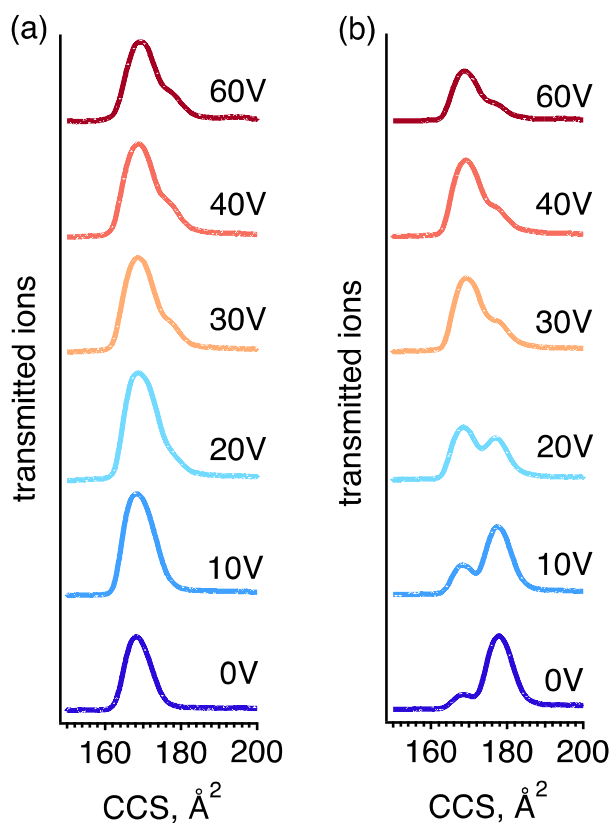


Figure 3. Collisional activation of $\text{BK}[1-5]^{2+}$ pre-selecting (a) peak I and (b) peak II in the drift-time distribution of Fig. 2. The color code corresponds to the activation voltage applied.

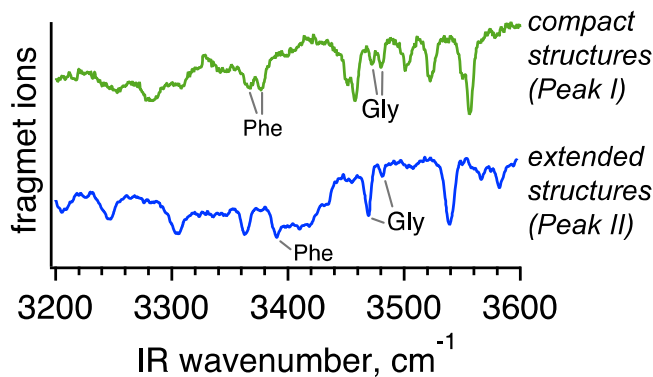


Figure 4. Vibrational spectra of mobility-selected $\text{BK}[1-5]^{2+}$. Phenylalanine and Glycine NH stretches are assigned by measuring the spectra of ^{15}N -labeled peptides.

3.2 IR-UV double resonance spectroscopy

One of the most powerful ways to simplify congested spectra of large molecules is to use double-resonance spectroscopy in a cryogenic ion trap.³⁸ We recorded vibrational spectroscopic signatures of three distinct conformers in our cold, octopole ion trap, shown in Fig. 5, and label them A, B and C. Isotopic labeling allows us to identify the NH stretches of the phenylalanine and glycine residues, which are labeled in Fig. 5. Note that the IR spectrum of conformer B is very close to that of conformer A, with the main difference being the frequencies of the phenylalanine NH stretch, which are separated by 27 cm^{-1} . This suggests that these two conformers differ in the rotation of phenylalanine side chain.^{82,83}

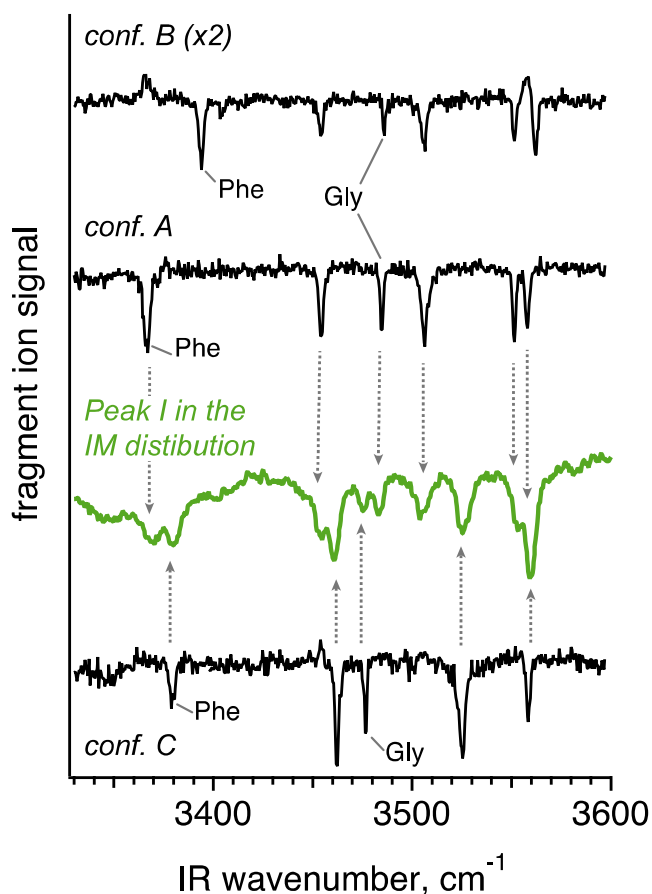


Figure 5. Comparison of vibrational spectra of 3 conformers (A, B and C) of $\text{BK}[1-5]^{2+}$ obtained in the CIS machine by IR-UV double-resonance together with a vibrational spectrum (in green) of the mobility-selected compact structures recorded in the IMS-CIS machine by H_2 -tagging. The low-CCS peak in the arrival-time distribution, accordingly, consists of a mixture of conformers A, C and, possibly, B. The labels show the NH-stretches that were assigned by measuring the spectra of ^{15}N -labeled peptide.

The spectra in Fig. 5 clearly demonstrate that peak I identified by ion mobility consists of conformers A and C. At the same time the spectroscopic differences between spectra of A and B are

1
2 so small that we cannot exclude presence of small quantities of conformer B. In the CIS instrument
3 that we currently use, ions undergo some collisional activation at the end of the ion funnel. This
4 explains why we observe a set of structures that largely resembles the annealed distribution obtained
5 in our IMS-CIS machine, i.e. mostly the compact structures. Despite the recent finding that H₂-
6 tagging can alter the conformation of small biological molecules,⁸⁴ in this case we observe that the
7 spectroscopic features are not detectably shifted when the peptide is tagged with one H₂ molecule.
8

9 To summarize the experimental results, the following structures are observed in the gas phase:
10

- 11 • The compact conformations with a CCS in the range of 167 to 170 Å². Analysis of their
12 spectral signatures suggests the presence of conformers A, B and C. B only differs from
13 A in the phenylalanine ring orientation. A third conformer, denoted C, is structurally
14 different from A and B.
15
- 16 • Extended structures with a CCS around 178 Å². They are kinetically trapped and upon
17 collisional activation collapse to the more stable compact conformations.
18
19

20 Previous studies of the full BK sequence suggest that families I and II differ by prolyl-peptide bond
21 isomers.^{42,85}
22
23
24

25 3.3 First-principles simulations

26 To determine the structures of the conformers that give rise to the CCS values and infrared
27 spectra that we measure, we have to compare these results with theory. First we must search the
28 massive conformational space for BK[1-5]²⁺ (discretization of the 13 single bonds in 60 degrees
29 steps and of the 4 peptide bonds to *cis* and *trans* states results in roughly 2×10^{11} structures to
30 evaluate). We tackle this sampling problem by a two-step approach: (i) a force field-based global
31 screening (basin hopping with Tinker and the OPLS-AA force field), and (ii) subsequent density-
32 functional theory calculations. In order to select the conformers to consider at the higher, first-
33 principles level, we employ experimental constraints, comparing the calculated CCS values and
34 vibrational signatures to their experimental counterparts. The use of experimental constraints is not
35 only a concession to the large conformational search space. Only one of the observed conformers
36 can be the global minimum of the potential-energy surface, while the rest, especially the kinetically
37 trapped species, cannot be determined based on the energy criterion alone.
38
39
40
41
42
43
44
45
46
47
48
49
50
51
52

53 The initial force field search yields 212,754 conformations that were sorted into 67,546 clusters,
54 the lowest energy representative of which was considered in the following. We first assumed, and
55 later confirmed, that kinetic trapping is a result of the *cis/trans* isomerization of the two prolyl-
56 peptide bonds present in BK[1-5]²⁺. All structures were categorized into four groups, *trans-trans*
57
58
59
60

(TT), *trans-cis* (TC), *cis-trans* (CT), and *cis-cis* (CC), according to their prolyl-peptide bond conformations. We have carried out the following analysis separately for each category so that we are sure to consider structures that are high in energy, such as TT, but that may still be observed experimentally due to kinetic trapping. We selected structures out of these individual sets based on their relative potential energy and calculated CCS. In order to put an emphasis on structures with CCSs that match the experiment, we applied an energy threshold of 30 kcal/mol relative to the lowest energy structure of the same backbone type to structures with CCS values between 165 Å² and 183 Å². For structures with a lower or higher CCS, we applied a relative energy threshold of 26 kcal/mol. By this procedure, we selected 4,515 structures that were subjected to geometry relaxations using the PBE functional with many-body dispersion correction and “light” computational settings.

3.3.1 Compact structures: Low-energy minima

To find candidates for the equilibrated stable structures of peak I, we rely mainly on the potential energy. First, the clustering procedure was applied to the initial pool of structures, and an energy threshold was used to select the structures to be optimized with “tight” settings. From these, we selected the lowest-energy structures in each proline configuration (TT, TC, CT or CC, 57 in total) and computed free energies and vibrational spectra in the harmonic approximation using the PBE functional and “tight” settings. Visual inspection of these spectra allowed us to choose the structures that best correspond to those we observed experimentally. We re-computed the spectra of all promising candidates using the PBE0 functional. The resulting spectra and the corresponding structures are shown in Fig. 6.

The calculated NH-stretch vibrational frequencies correspond remarkably well to the measured frequencies, including the hydrogen-bonded NH stretches. However, we observe a systematic shift between calculated and experimental frequencies of the free OH stretch vibration. Such a discrepancy can result from (i) the possible incomplete inclusion of electron exchange and correlation and (ii) the use of a single scale factor to globally account for vibrational anharmonicity and nuclear quantum effects.⁸⁶ The former issue is resolved by the use of the PBE0 hybrid functional with exact Hartree-Fock exchange. Provided a large data set of computed vs experimentally measured vibrational frequencies is available, the latter could be resolved by finding scaling factors for each vibrational mode by linear regression and subsequently using them for a system with unknown geometry. With this approach, it has been shown that these factors differ between NH and OH stretches.⁸⁷ In the absence of such a data set, we use a single scale factor to

1
2 account for vibrational anharmonicity. In light of this, it is not surprising that the calculated OH
3 vibrational band is shifted from experiment, since the scale factor is largely determined by the
4 agreement for the more numerous NH stretch bands. Routes towards a correct simulation of the
5 experimental OH stretch peak positions without the need for scaling are known – simulations that
6 fully include anharmonic effects and a quantum mechanical treatment of the nuclear motions.
7 Examples are the multi-configurational time-dependent Hartree method⁸⁸ or the approximate
8 thermostatted ring-polymer molecular dynamics method.⁸⁹ However, such methodology is not yet
9 straightforwardly applicable to molecules of the size investigated here.

10
11 As shown in Fig. 6, we were able to assign structures that fit to the spectral signatures that we
12 found in peak I of the CCS distribution. Conformers A and B differ by the orientation of the
13 phenylalanine ring, as the experimental data suggest. Conformers A and C have different
14 configurations: in A the prolines are in a *cis-trans* configuration, while in C they are *trans-cis*.
15 Despite the difference in structure, their calculated CCS values are very close: 169 Å² and 168 Å².

16
17 We measure ion mobilities at room temperature and then cool the ions in the cold ion trap.
18 Depending on the rate of cooling, one might expect a certain degree of re-equilibration of the
19 conformational distribution in this process. If the cooling is fast with respect to the isomerization
20 rate between conformers, kinetic trapping can occur, preventing the preferred geometries at 300 K
21 from converting to the low-energy, gas-phase structures at low temperature. In order to gain insight
22 into the dependence of the energy ordering of the different conformations on the temperature of the
23 molecule, we computed the energies of all 57 candidates with the PBE0 functional and then
24 evaluated the free energy for a range of temperatures using a harmonic approximation. Figure 7
25 shows how the relative energies change within the CT, TC and CC categories for 3 cases: pure
26 potential energy (i.e., 0 K), free energy at 10 K, and free energy at 300 K. The importance of the
27 free energy correction can be demonstrated using the example of the conformation that corresponds
28 to the global minimum on the potential-energy surface (PES). It is a very compact CT structure
29 with a CCS of 157 Å² and is not observed in the experiment. Indeed, at 300 K this conformer no
30 longer represents the global minimum.
31
32
33
34
35
36
37
38
39
40
41
42
43
44
45
46
47
48
49
50
51
52
53
54
55
56
57
58
59
60

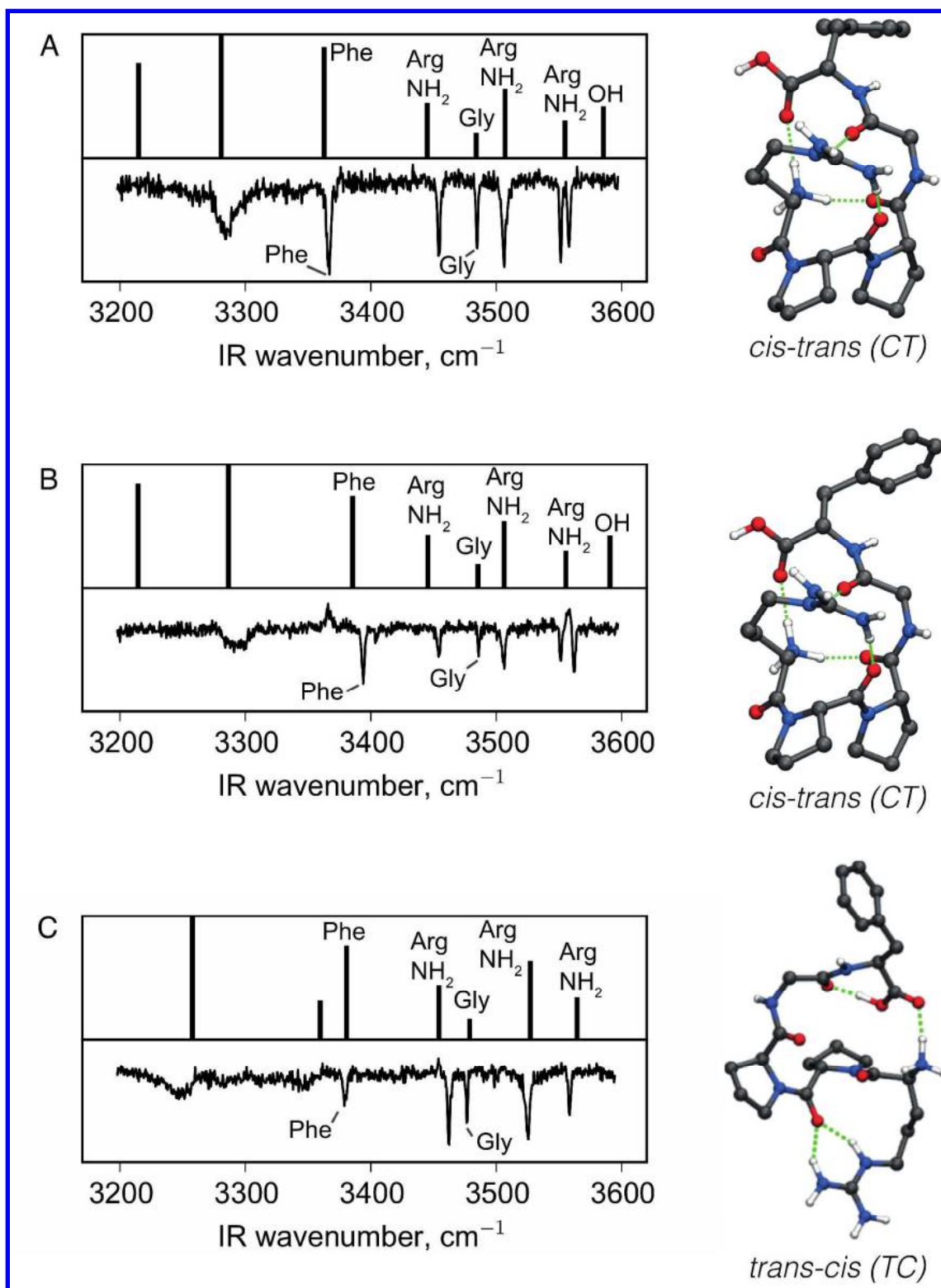


Figure 6. Comparison between calculated and experimental spectra for conformers A, B and C, forming peak I. The corresponding structures are shown and the conformation of prolyl-peptide bonds is noted for each conformer. The NH stretch vibrations in the experimental spectra are identified via isotopic labeling. For the computed spectra all relevant local modes are labeled.

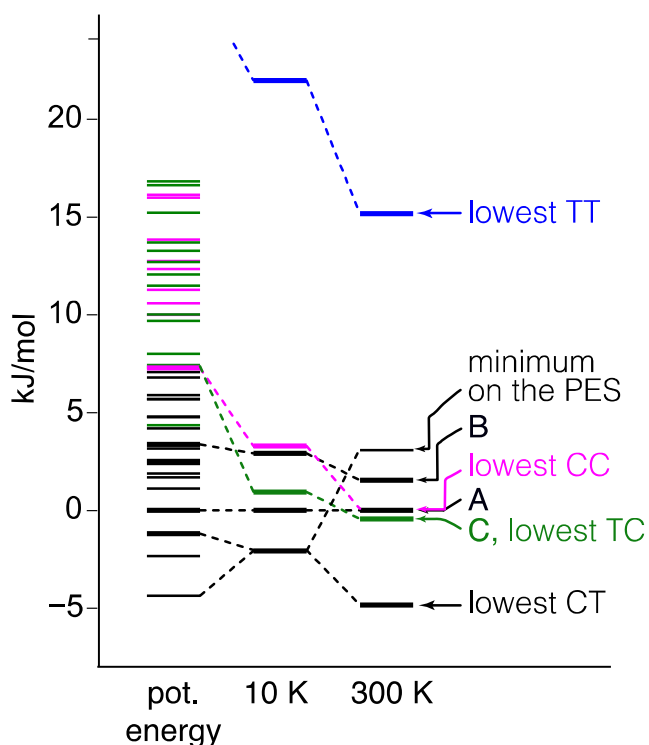


Figure 7. On the left: relative potential energies within CT (black), TC (green) and CC (magenta) configurations. On the right: the change in relative energies of the main conformers for 3 cases: pure potential energy, free energy at 10 K and free energy at 300 K. A, B and C label the experimentally observed conformations. The lowest energy TT structure (blue) is given for a reference. The lowest-energy geometries at 300 K for TC, CT and CC configurations are labeled as well.

The energy difference at 300 K between conformer A and the global minimum is within 0.6 meV per atom, which is at the limit of what can be resolved at this level of theory. The global minimum at 300 K (GM 300 K in Table 1) is a CT structure that has the same hydrogen bonding pattern as A and B but which differs from them mainly by rotation of the phenyl ring (see SI-Fig. 3). A number of other low-energy structures at 300 K with similar H-bonding patterns and CCS as A and B have been identified. We speculate that at 300 K the structures of the CT type are close to the global minimum and are rapidly interconverting, while after cooling the ions in the trap we freeze out mainly conformer A and traces of conformer B. The higher the number of similar structures available around the global minimum, the higher is the volume of conformational space corresponding to this basin at 300 K and, accordingly, the higher is the probability to find the molecule there.

Note that conformer C is the lowest-energy structure in the TC category at 300 K. In general, we observe in the experiment the low-energy geometries for CT and TC types but not of the CC type. Further computations of energy barriers between different conformers are needed to fully

1
2 understand why only a fraction of the available low-energy structures is observed experimentally. It
3 could also lead to a better understanding of the interplay between the collisional cooling rate and the
4 isomerization rate.
5
6

7 8 **3.3.2 Extended kinetically trapped structures** 9

10 While there is a relatively well-established (though computationally expensive) procedure for
11 searching for the global minimum on a potential energy surface, identifying kinetically trapped
12 conformations is challenging. One cannot rely on the energy criterion, because the kinetically
13 trapped structures lie, by definition, high in energy and are separated from other conformational
14 basins with even higher energy barriers. In this case, experimental constraints play a key role in
15 guiding quantum-chemical calculations. One of them is the CCS. We computed CCSs of all
16 geometries in the initial pool of structures, and as shown in Fig. 8(a), we considered only those that
17 have CCS higher than 176 \AA^2 , which means they fall under peak II in the arrival-time distribution.
18 The energy threshold for a structure to be considered was kept as high as possible: 48 kJ/mol (0.5
19 eV) from the lowest-energy conformer in each type. We calculated vibrational spectra at the
20 PBE+MBD level for all structures that satisfied these two conditions (135 in total). This enabled a
21 second selection step, apart from the CCS cutoff, based on spectroscopic information:
22
23
24
25
26
27
28
29
30

- 31 1. In the IR spectrum of extended structures (see Fig. 4) there are two bands above 3570 cm^{-1} .
32 The only vibration in this molecule that can have such high frequency is OH stretch,
33 suggesting that there at least two conformers under the peak II of the drift-time distribution
34 and each of them has a free OH stretch.
35
36
37
- 38 2. In the IR spectrum of conformational family II there is a unique, intense band at 3538 cm^{-1} ,
39 which is too high for a backbone NH vibration and thus corresponds to the side chain of
40 arginine.⁸³ To decide if this side chain interacts with other parts of the molecule, we
41 compare its spectroscopic signature with those of conformers A, B and C. Their spectra
42 show that the asymmetric stretch of a *free* η -NH₂ of arginine appears at a frequency higher
43 than 3540 cm^{-1} while the symmetric stretch occurs between 3450 cm^{-1} and 3500 cm^{-1} . Since
44 the intense band in the spectrum of peak II (see Fig. 4) is slightly lower than this, we
45 conclude that the extended conformers have no free η -NH₂ groups, but a least one weakly
46 interacting with other parts of the molecule.
47
48
49
50
51
- 52 3. The free ϵ -NH stretch of arginine should appear on 3465 cm^{-1} .^{90,91} The absence of this
53 band in the spectrum suggests that the ϵ -NH of arginine in all the extended conformers is
54 hydrogen bonded.
55
56
57
58
59
60

4. The strong bands at 3362 cm^{-1} and 3303 cm^{-1} are most probably the spectroscopic signature of the free NH_3^+ group or one weakly bound to a phenyl ring.⁹²
5. Based on the comparison with the spectra of conformers A, B and C, the phenylalanine NH stretch might interact with the phenyl ring, while the NH stretch of glycine appears to be free.

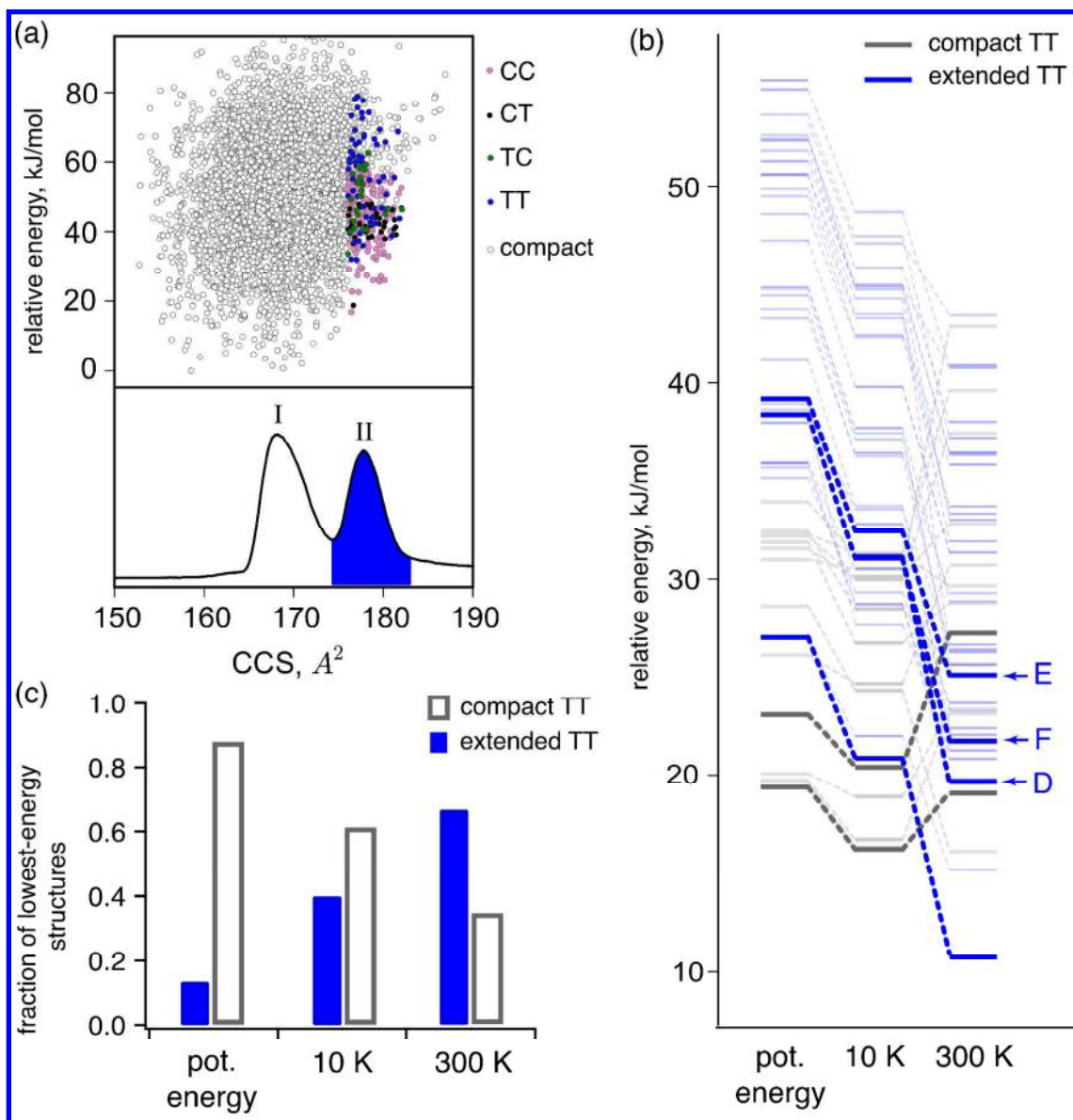


Figure 8. (a) Distribution of relative potential energies of considered conformers as a function of CCS. Those conformations for which the vibrational spectra were computed are shown in color. The rest of the structures are shown in grey. (b) Energy hierarchy for the lowest-energy structures of TT type. The extended structures with CCS higher than 176 \AA^2 are shown in blue, the compact ones – in grey. The structures that are found in the experiment and several representative low-energy structures are highlighted to show the general trend. (c) The ratio between compact and extended (CCS higher than 176 \AA^2) structures among 15 lowest-energy conformers without and with temperature correction.

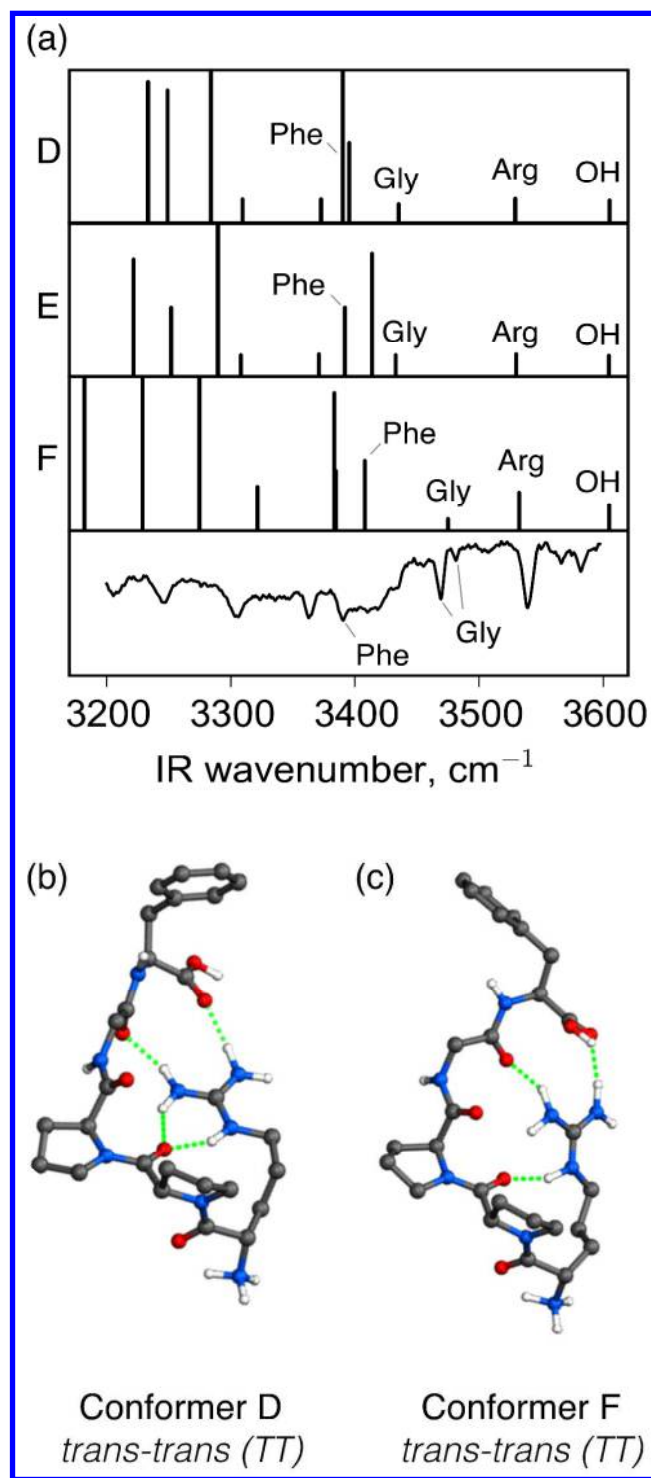


Figure 9. (a) Calculated vibrational spectra of conformers D, E and F compared to the experimental spectrum of peak II of the arrival-time distribution; (b), (c) the corresponding structures. Structure of the conformer E is visually almost indistinguishable from the conformer D and is not shown.

With these considerations we aim to rationalize the comparison between experimental and simulated spectra that otherwise is easily prone to incorrect or non-precise assignment. It is necessary to analyze the spectroscopic features manually and to perform isotopic labeling. After

1
2 applying the criteria stated above to the simulated spectra and molecular geometries, only structures
3 of type TT remain, meaning that both prolyl peptide bonds are in the *trans* configuration. We re-
4 computed the IR spectra of those structures that satisfy the above criteria with the PBE0 functional,
5 which further improved the agreement between simulated and experimental vibrational spectra (Fig.
6 9(a)).
7
8

9
10
11 Figures 8 (b) and (c) explain why we observe elongated TT structures in the ion mobility
12 experiment. They are more stable at 300 K than the compact structures, while the latter become
13 more energetically favorable at 10 K. At 300 K the elongated structures traverse the drift tube,
14 rapidly interconverting between the close minima on the free energy surface. Then they are
15 transferred to the cold ion trap, where the final structure at 10 K results from the interplay between
16 collisional cooling and isomerization. The fact that we observe spectroscopically the elongated
17 structures suggests that some of their features are preserved in the cooling process. Kinetic trapping
18 could occur twice during their transition from solution to our cold ion trap: in the ion source and in
19 the cryogenic ion trap. We observe evidence of some kinetic trapping in both cases.
20
21
22
23
24
25
26

27 **4 Discussion: Overview of the conformational space of bradykinin 1-** 28 29 **5** 30 31

32 Numerous NMR studies of the full bradykinin molecule indicate that in aqueous solution it
33 mainly adopts an all-*trans* conformation,^{10-12,14-16} which is consistent with the *trans* bond being
34 slightly more stable than *cis* in polar environments due to its higher dipole moment.¹¹ Two receptors
35 of bradykinin are known,⁹³ B1 and B2, and in the complex with the B2 receptor bradykinin is in the
36 all-*trans* form.^{13,15} If the medium becomes non-polar, alternative backbone conformations involving
37 *cis* prolyl peptide bonds are more competitive.⁹⁴ The transfer to the gas phase has a similar effect on
38 its structure as the transfer to a non-polar solvent or interaction with a membrane: the conformations
39 involving this *cis*-configuration of prolyl-peptide bonds become more stable.
40
41
42
43
44

45
46 We observe the same type of behavior for BK[1-5]²⁺, which acts *in vivo* as an inhibitor of
47 thrombin. An X-ray structure of the complex demonstrates that all peptide bonds in BK[1-5] remain
48 *trans*.⁵⁵ We performed NMR measurements in a CD₃OH:H₂O mixture, which reproduces the solvent
49 used for the ESI experiments. Peaks were assigned using COSY and TOCSY 2D ¹H spectra with
50 water suppression, and the assignments are supported by comparison with spectra acquired in
51 DMSO, where no background water signal hinders the cross-peaks. No residual secondary structure
52 is identified based on the H α secondary chemical shifts, which are close to zero for all residues but
53 N-terminal arginine (see Table 1 in the SI).^{95,96} The ROESY 2D ¹H NMR spectrum shows that 82%
54
55
56
57
58
59
60

of molecules in a 50:50 water/methanol mixture adopt the *trans-trans* configuration (see SI-Figure 1). Three alternative conformers do not have a fully resolved spin system and thus it is difficult to identify them.

Upon electrospraying from the same water/methanol mixture, we observe a kinetically trapped conformational family in which all the bonds remain *trans*. These TT conformers are folded in such a way that the N-terminus of the molecule remains free, while the arginine side chain interacts with the C=O groups of the backbone. The broad ion-mobility peak reflects the disordered behavior in solution. Inside the drift tube at room temperature closely related conformations might be rapidly interconverting, while at 10 K in the conditions of the cold ion trap the structure becomes well defined. We do not observe the lowest-energy structures of the TT type in the experiment, but rather the ones that lie quite high in energy. This means that the mechanism of kinetic trapping involves not only *cis-trans* isomerization, but also H-bond rearrangement, which can have high-energy barriers as well.

Table 1. Comparison of the major conformers identified in the present study. GM denotes the global minimum on the corresponding energy surface.

Conf.	Prolyl-peptide bond conformation	Potential energy, meV ^a	Free energy at 10 K, meV ^a	Free energy at 300 K, meV ^a	CCS experiment, Å ²	CCS computed, Å ²
GM (pot)	CT	-45	-21	32	-	157
GM(10 K)	CT	12	-24	-36	-	165
GM(300 K)	CT	-12	-21	-50	-	168
A	CT	0	0	0	167, 170	169
B	CT	35	30	16	167, 170	169
C, lowest TC (10 K and 300 K)	TC	76	10	-5	167, 170	171
Lowest TT (300 K)	TT	280	216	111	-	175
D	TT	394	322	204	178	177
E	TT	406	336	260	178	176
F	TT	398	322	225	178	177
Lowest CC	CC	75	34	1	-	169

^a Relative to conformer A.

Upon collisional activation, TT conformers of BK[1-5]²⁺ (i.e., the extended structures in the IM distribution) convert to TC and CT structures (the compact ones). The relative abundances of these conformers at different degrees of activation observed by cryogenic ion spectroscopy (see SI-Fig. 2) suggest that first the TT to TC transition occurs, followed by TT to CT. The alternative pathway *via* CC conformers is unlikely as we do not find any trace of CC conformers, even though their free energies are close to those of conformers A and C. Further investigation of conversion paths

1
2 between all types of structures will shed light on this issue. One explanation might be that the
3 barrier height between CC and the rest of the conformational space is significantly higher than
4 between TT and CT or TT and TC, so that the molecule fragments before sampling the CC states.
5
6

7 In all cases except TT, the N-terminus and arginine side chain can both form H-bonds, which
8 stabilize the molecule compared to TT. The external hydrogen bonds have to be substituted by
9 internal ones upon the removal of water. This is why in the gas phase even the lowest-energy TT
10 structure is significantly less stable than TC, CT and CC (Table 1). These latter three types have
11 compact low-energy structures with CCSs falling within peak I in the drift-time distribution. Low-
12 energy conformers of the TT type tend to be more extended, with CCSs close to peak II in the drift-
13 time distribution. Overall, the calculated CCSs presented in Table 1 agree well with the values that
14 we measure, given that the experimental error is estimated to be around 2 \AA^2 . The compaction in the
15 gas phase corresponds to the effect observed for BK adhered to the surface of a micelle.⁹⁷
16
17
18
19
20
21
22

23 5 Conclusion

24 The combination of ion mobility and cryogenic ion spectroscopy has allowed us to characterize
25 all major conformations of $\text{BK}[1-5]^{2+}$ in the gas phase. While only two well-resolved peaks are
26 separated by ion mobility, we show spectroscopically that there are several conformers within each
27 of them. Our calculations reveal that three very different conformational families (*cis-trans*, *trans-*
28 *cis* and *cis-cis*) have close free energies and CCSs in the gas phase, and, by combining the
29 experimental spectroscopic information with first-principles simulation data, we were able to assign
30 them. We determine that the lowest-energy gas-phase structures of the peptide feature backbone
31 conformations with the two prolyl-peptide bonds in either *cis-trans* or *trans-cis* state. Both of them
32 fall within the more compact ion mobility peak at 167 to 170 \AA^2 .
33
34
35
36
37
38
39
40
41

42 Kinetic trapping can occur at different points in the “life cycle” of the ion in our instrument.
43 First, when the ions are initially desolvated in the electrospray, the conformations coming out of
44 solution can be kinetically trapped behind barriers that result from internal hydrogen bonding and
45 separation in *cis-trans* states of the prolyl-peptide bonds. Second, if cold-ion spectroscopy is used,
46 kinetic trapping can occur when cooling the molecules. In this case, when the collisional cooling
47 rate is faster than the isomerization rate, the population of conformers that are higher in energy than
48 the global minimum can be trapped behind isomerization barriers.
49
50
51
52
53

54 We have identified the kinetically trapped conformers of $\text{BK}[1-5]^{2+}$ as all-*trans*, which is the
55 predominant backbone conformation type in solution. This provides the basis for further gas-phase
56 studies to investigate the isomerization barriers between the prolyl-peptide bond types CC, CT, TC,
57
58
59
60

1
2 and TT and to study the extent of micro-solvation that is required to render TT more stable than the
3 alternative backbone types. The width of the observed IM peak and the spectroscopic signature of
4 the kinetically trapped conformations suggest a wide variety of structures, which is in agreement
5 with the intrinsic disorder in solution. In stark contrast to this, we have shown that the stable, gas-
6 phase *cis-trans* and *trans-cis* conformers appear to represent well-defined minima. This is
7 consistent with the notion that disordered peptides collapse to particular secondary structure in non-
8 polar media such as cell membranes.
9
10
11
12
13

14 **6 Acknowledgements**

15
16 We are grateful to the EPFL, the Swiss National Science Foundation (grant number
17 200020_152804) and the joint EPFL-Max Planck Center for Molecular Nanotechnology for the
18 financial support of this work. The authors also thank Dr. Pascal Mieville and Dr. Luc Patiny for
19 the NMR data. CB thanks Dr. Mariana Rossi for sharing her knowledge about theoretical vibrational
20 spectroscopy and Prof. Matthias Scheffler for his continuous support.
21
22
23
24
25
26

27 **7 Supporting information**

28
29 ROESY NMR spectrum of bradykinin 1-5 in DMSO and CD₃OH:H₂O solutions; table of
30 secondary chemical shifts of bradykinin 1-5 in CD₃OH:H₂O solution, vibrational spectrum of
31 annealed conformational distribution of bradykinin 1-5; the structure of lowest-energy conformer of
32 bradykinin 1-5 in the gas phase. This material is available free of charge via the Internet at
33 <http://pubs.acs.org>.
34
35
36
37
38
39
40
41
42
43
44
45
46
47
48
49
50
51
52
53
54
55
56
57
58
59
60

8 References

- (1) Uversky, V. N.; Dunker, A. K. *Biochim. Biophys. Acta* **2010**, *1804*, 1231-1264.
- (2) Turoverov, K. K.; Kuznetsova, I. M.; Uversky, V. N. *Prog. Biophys. Mol. Biol.* **2010**, *102*, 73-84.
- (3) Kaltashov, I. A.; Eyles, S. J. In *Mass Spectrometry in Biophysics: Conformation and Dynamics of Biomolecules*; John Wiley & Sons: Hoboken, NJ, 2005; pp 45-86.
- (4) Mittag, T.; Forman-Kay, J. D. *Curr. Opin. Chem. Biol.* **2007**, *17*, 3-14.
- (5) Jensen, M. R.; Markwick, P. R.; Meier, S.; Griesinger, C.; Zweckstetter, M.; Grzesiek, S.; Bernado, P.; Blackledge, M. *Structure* **2009**, *17*, 1169-1185.
- (6) Henzler-Wildman, K.; Kern, D. *Nature* **2007**, *450*, 964-972.
- (7) Gibbs, E. B.; Showalter, S. A. *Biochemistry* **2015**, *54*, 1314-1326.
- (8) Dunker, A. K.; Silman, I.; Uversky, V. N.; Sussman, J. L. *Curr. Opin. Struct. Biol.* **2008**, *18*, 756-764.
- (9) Regoli, D.; Barabe, J. *Pharmacol. Rev.* **1980**, *32*, 1-46.
- (10) Richard, T.; Vergé, S.; Berké, B.; Vercauteren, J.; Monti, J. P. *J. Biomol. Struct. Dyn.* **2001**, *18*, 627-637.
- (11) Young, J. K.; Hicks, R. P. *Biopolymers* **1994**, *34*, 611-623.
- (12) Gaggelli, E.; D'Amelio, N.; Maccotta, A.; Valensin, G. *Eur. J. Biochem.* **1999**, *262*, 268-276.
- (13) Lopez, J. J.; Shukla, A. K.; Reinhart, C.; Schwalbe, H.; Michel, H.; Glaubitz, C. *Angew. Chem. Int. Ed.* **2008**, *47*, 1668-1671.
- (14) Glover, M. S.; Bellinger, E. P.; Radivojac, P.; Clemmer, D. E. *Anal. Chem.* **2015**, *87*, 8466-8472.
- (15) Otteleben, H.; Haasemann, M.; Ramachandran, R.; Gorchach, M.; MullerEsterl, W.; Brown, L. R. *Eur. J. Biochem.* **1997**, *244*, 471-478.
- (16) Kaminski, G. A.; Friesner, R. A. *J. Phys. Chem. B* **2001**, *105*, 6474-6487.
- (17) Richard, T.; Delaunay, J. C.; Mérillon, J. M.; Monti, J. P. *J. Biomol. Struct. Dyn.* **2003**, *21*, 379-385.
- (18) Bonechi, C.; Ristori, S.; Martini, G.; Martini, S.; Rossi, C. *Biochim. Biophys. Acta* **2009**, *1788*, 708-716.
- (19) Gothel, S. F.; Marahiel, M. A. *CMLS* **1999**, *55*, 423-436.
- (20) Fanghänel, J. r.; Fischer, G. *Front. Biosci.* **2004**, *9*, 3453-3478.
- (21) Nigro, P.; Pompilio, G.; Capogrossi, M. C. *Cell Death Dis.* **2013**, *4*, e888.
- (22) Satoh, K.; Matoba, T.; Suzuki, J.; O'Dell, M. R.; Nigro, P.; Cui, Z.; Mohan, A.; Pan, S.; Li, L.; Jin, Z.-G.; Yan, C.; Abe, J.-i.; Berk, B. C. *Circulation* **2008**.
- (23) Zoldák, G.; Aumüller, T.; Lücke, C.; Hritz, J.; Oostenbrink, C.; Fischer, G.; Schmid, F. *X. Biochemistry* **2009**, *48*, 10423-10436.
- (24) Kunz, C.; Jahreis, G.; Gunther, R.; Berger, S.; Fischer, G.; Hofmann, H. J. *J. Pept. Sci.* **2012**, *18*, 400-404.
- (25) Baldauf, C.; Pagel, K.; Warnke, S.; von Helden, G.; Kokscho, B.; Blum, V.; Scheffler, M. *Chem. - Eur. J.* **2013**, *19*, 11224-11234.
- (26) Warnke, S.; Baldauf, C.; Bowers, M. T.; Pagel, K.; von Helden, G. *J. Am. Chem. Soc.* **2014**, *136*, 10308-10314.
- (27) Valiaev, A.; Lim, D. W.; Oas, T. G.; Chilkoti, A.; Zauscher, S. *J. Am. Chem. Soc.* **2007**, *129*, 6491-6497.
- (28) Zhang, X.; Halvorsen, K.; Zhang, C.-Z.; Wong, W. P.; Springer, T. A. *Science* **2009**, *324*, 1330-1334.

- 1
2 (29) Chen, J.; Edwards, S. A.; Gräter, F.; Baldauf, C. *J. Phys. Chem. B* **2012**, *116*, 9346-
3 9351.
4 (30) Beveridge, R.; Phillips, A. S.; Denbigh, L.; Saleem, H. M.; MacPhee, C. E.; Barran, P.
5 *E. Proteomics* **2015**, *15*, 2872-2883.
6 (31) Buchberger, A.; Yu, Q.; Li, L. *Annu Rev Anal Chem* **2015**, *8*, 485-509.
7 (32) Schennach, M.; Breuker, K. *J. Am. Soc. Mass. Spectrom.* **2015**, *26*, 1059-1067.
8 (33) Boeri Erba, E.; Petosa, C. *Protein Sci.* **2015**, *24*, 1176-1192.
9 (34) Konermann, L.; Vahidi, S.; Sowole, M. A. *Anal. Chem.* **2014**, *86*, 213-232.
10 (35) Wyttenbach, T.; Pierson, N. A.; Clemmer, D. E.; Bowers, M. T. *Annu. Rev. Phys.*
11 *Chem.* **2014**, *65*, 175-196.
12 (36) Stedwell, C. N.; Galindo, J. F.; Roitberg, A. E.; Polfer, N. C. *Annu. Rev. Anal. Chem.*
13 **2013**, *6*, 267-285.
14 (37) Balasubramaniam, D.; Komives, E. *Biochim. Biophys. Acta* **2012**, *1834*, 1202-
15 1209.
16 (38) Rizzo, T. R.; Stearns, J.; Boyarkin, O. V. *Int. Rev. Phys. Chem.* **2009**, *28*, 481-515.
17 (39) Baldauf, C.; Rossi, M. *J. Phys.: Condens. Matter* **2015**, *27*, 493002.
18 (40) Wyttenbach, T.; Helden, G. V.; Bowers, M. T. *J. Am. Chem. Soc.* **1996**, *118*, 8355-
19 8364.
20 (41) Pierson, N. A.; Chen, L.; Valentine, S. J.; Russell, D. H.; Clemmer, D. E. *J. Am. Chem.*
21 *Soc.* **2011**, *133*, 13810-13813.
22 (42) Pierson, N. A.; Chen, L.; Russell, D. H.; Clemmer, D. E. *J. Am. Chem. Soc.* **2013**, *135*,
23 3186-3192.
24 (43) Bohrer, B. C.; Merenbloom, S. I.; Koeniger, S. L.; Hilderbrand, A. E.; Clemmer, D. E.
25 *Annu. Rev. Anal. Chem.* **2008**, *1*, 293-327.
26 (44) Chen, S. H.; Russell, D. H. *J. Am. Soc. Mass. Spectrom.* **2015**, *26*, 1433-1443.
27 (45) Papadopoulos, G.; Svendsen, A.; Boyarkin, O. V.; Rizzo, T. R. *J. Am. Soc. Mass.*
28 *Spectrom.* **2012**, *23*, 1173-1181.
29 (46) Pierson, N. A.; Clemmer, D. E. *Int. J. Mass spectrom.* **2015**, *377*, 646-654.
30 (47) Silveira, J. A.; Fort, K. L.; Kim, D.; Servage, K. A.; Pierson, N. A.; Clemmer, D. E.;
31 Russell, D. H. *J. Am. Chem. Soc.* **2013**, *135*, 19147-19153.
32 (48) van der Spoel, D.; Marklund, E. G.; Larsson, D. S. D.; Caleman, C. *Macromol. Biosci.*
33 **2011**, *11*, 50-59.
34 (49) Breuker, K.; McLafferty, F. W. *Proc. Natl. Acad. Sci. USA* **2008**, *105*, 18145-18152.
35 (50) Breuker, K.; Brüscheiler, S.; Tollinger, M. *Angew. Chem. Int. Ed.* **2011**, *50*, 873-
36 877.
37 (51) Shelimov, K. B.; Jarrold, M. F. *J. Am. Chem. Soc.* **1997**, *119*, 2987-2994.
38 (52) Kjaergaard, M. *Intrinsically Disord. Proteins* **2015**, *3*, 1-7.
39 (53) Murphey, L. J.; Hatchey, D. L.; Oates, J. A.; Morrow, J. D.; Brown, N. J. *The Journal*
40 *of Pharmacology and Experimental Therapeutics* **2000**, *294*, 263-269.
41 (54) Morinelli, T. A.; Webb, J. G.; Jaffa, A. A.; Privitera, P. J.; Margolius, H. S. *J.*
42 *Pharmacol. Exp. Ther.* **2001**, *296*, 71-76.
43 (55) Hasan, A. A. K.; Warnock, M.; Nieman, M.; Srikanth, S.; Mahdi, F.; Krishnan, R.;
44 Tulinsky, A.; Schmaier, A. H. *Am. J. Physiol. Heart Circ. Physiol.* **2003**, *285*, 183-193.
45 (56) Nieman, M. T.; Pagan-Ramos, E.; Warnock, M.; Krijanovski, Y.; Hasan, A. A. K.;
46 Schmaier, A. H. *FEBS Lett.* **2005**, *579*, 25-29.
47 (57) Sawyer, H. a.; Marini, J. T.; Stone, E. G.; Ruotolo, B. T.; Gillig, K. J.; Russell, D. H. *J.*
48 *Am. Soc. Mass. Spectrom.* **2005**, *16*, 893-905.
49
50
51
52
53
54
55
56
57
58
59
60

- (58) Svendsen, A.; Lorenz, U. J.; Boyarkin, O. V.; Rizzo, T. R. *Rev. Sci. Instrum.* **2010**, *81*, 073107.
- (59) Masson, A.; Kamrath, M. Z.; Perez, M. A.; Glover, M. S.; Rothlisberger, U.; Clemmer, D. E.; Rizzo, T. R. *J. Am. Soc. Mass. Spectrom.* **2015**, *26*, 1444-1454.
- (60) Koeniger, S. L.; Merenbloom, S. I.; Valentine, S. J.; Jarrold, M. F.; Udseth, H. R.; Smith, R. D.; Clemmer, D. E. *Anal. Chem.* **2006**, *78*, 4161-4174.
- (61) Kamrath, M. Z.; Garand, E.; Jordan, P. A.; Leavitt, C. M.; Wolk, A. B.; Van Stipdonk, M. J.; Miller, S. J.; Johnson, M. A. *J. Am. Chem. Soc.* **2011**, *133*, 6440-6448.
- (62) Nagornova, N. S.; Rizzo, T. R.; Boyarkin, O. V. *Angew. Chem. Int. Ed.* **2013**, *52*, 6002-6005.
- (63) Kelly, R. T.; Tolmachev, A. V.; Page, J. S.; Tang, K.; Smith, R. D. *Mass Spectrom. Rev.* **2010**, *29*, 294-312.
- (64) Pappu, R. V.; Hart, R. K.; Ponder, J. W. *J. Phys. Chem. B* **1998**, *102*, 9725-9742.
- (65) Van Der Spoel, D.; Lindahl, E.; Hess, B.; Groenhof, G.; Mark, A. E.; Berendsen, H. J. *C. J. Comput. Chem.* **2005**, *26*, 1701-1718.
- (66) Hess, B.; Kutzner, C.; van der Spoel, D.; Lindahl, E. *J. Chem. Theory Comput.* **2008**, *4*, 435-447.
- (67) Wyttenbach, T.; Helden, G.; Batka, J. J.; Carlat, D.; Bowers, M. T. *J. Am. Soc. Mass. Spectrom.* **1997**, *8*, 275-282.
- (68) https://labs.chem.ucsb.edu/bowers/michael/theory_analysis/cross-sections/sigma.shtml.
- (69) Mesleh, M. F.; Hunter, J. M.; Shvartsburg, A. A.; Schatz, G. C.; Jarrold, M. F. *J. Phys. Chem.* **1996**, *100*, 16082-16086.
- (70) <http://www.indiana.edu/~nano/software/>.
- (71) Blum, V.; Gehrke, R.; Hanke, F.; Havu, P.; Havu, V.; Ren, X.; Reuter, K.; Scheffler, M. *Comput. Phys. Commun.* **2009**, *180*, 2175-2196.
- (72) Perdew, J. P.; Burke, K.; Ernzerhof, M. *Phys. Rev. Lett.* **1996**, *77*, 3865-3868.
- (73) DiStasio, R. A.; von Lilienfeld, O. A.; Tkatchenko, A. *Proc. Natl. Acad. Sci. USA* **2012**, *109*, 14791-14795.
- (74) Tkatchenko, A.; DiStasio, R. A.; Car, R.; Scheffler, M. *Phys. Rev. Lett.* **2012**, *108*, 1-5.
- (75) Adamo, C.; Barone, V. *J. Chem. Phys.* **1999**, *110*, 6158-6158.
- (76) Rossi, M.; Chutia, S.; Scheffler, M.; Blum, V. *J. Phys. Chem. A* **2014**, *118*, 7349-7359.
- (77) Schubert, F.; Pagel, K.; Rossi, M.; Warnke, S.; Salwiczek, M.; Kokschi, B.; von Helden, G.; Blum, V.; Baldauf, C.; Scheffler, M. *Phys. Chem. Chem. Phys.* **2015**, *17*, 5376-5385.
- (78) Schubert, F.; Rossi, M.; Baldauf, C.; Pagel, K.; Warnke, S.; von Helden, G.; Filsinger, F.; Kupser, P.; Meijer, G.; Salwiczek, M.; Kokschi, B.; Scheffler, M.; Blum, V. *Phys. Chem. Chem. Phys.* **2015**, *17*, 7373-7385.
- (79) <http://mestrelab.com/software/mnova/nmr/>.
- (80) Pierson, N. A.; Valentine, S. J.; Clemmer, D. E. *J. Phys. Chem. B* **2010**, *114*, 7777-7783.
- (81) Voronina, L.; Rizzo, T. R. *Phys. Chem. Chem. Phys.* **2015**, *17*, 25828-25836.
- (82) Stearns, J.; Seaiby, C.; Boyarkin, O. V.; Rizzo, T. R. *Phys. Chem. Chem. Phys.* **2009**, *11*, 125-132.
- (83) Zabuga, A. V.; Rizzo, T. R. *J. Phys. Chem. Lett.* **2015**, *6*, 1504-1508.
- (84) Masson, A.; Williams, E. R.; Rizzo, T. R. *J. Chem. Phys.* **2015**, *143*, 104313.
- (85) Morrison, L. J.; Wysocki, V. H. *Int. J. Mass spectrom.* **2015**, *391*, 2-10.

- 1
2 (86) Scott, A. P.; Radom, L. *J. Phys. Chem.* **1996**, *100*, 16502-16513.
3 (87) Bouteiller, Y.; Gillet, J.-C.; Grégoire, G.; Schermann, J. P. *J. Phys. Chem. A* **2008**, *112*,
4 11656-11660.
5 (88) Vendrell, O.; Gatti, F.; Meyer, H.-D. *J. Chem. Phys.* **2007**, *127*, 184303.
6 (89) Rossi, M.; Ceriotti, M.; Manolopoulos, D. E. *J. Chem. Phys.* **2014**, *140*, 234116.
7 (90) Bush, M. F.; O'Brien, J. T.; Prell, J. S.; Saykally, R. J.; Williams, E. R. *J. Am. Chem. Soc.*
8 **2007**, *129*, 1612-1622.
9 (91) Polfer, N. C.; Oomens, J. *Mass Spectrom. Rev.* **2009**, *28*, 468-494.
10 (92) Chiavarino, B.; Crestoni, M. E.; Schutz, M.; Bouchet, A.; Piccirillo, S.; Steinmetz, V.;
11 Dopfer, O.; Fornarini, S. *J. Phys. Chem. A* **2014**, *118*, 7130-7138.
12 (93) Takano, M.; Matsuyama, S. *Eur. J. Pharmacol.* **2014**, *732*, 169-172.
13 (94) Cann, J. R.; Liu, X.; Stewart, J. M.; Gera, L.; Kotovych, G. *Biopolymers* **1994**, *34*,
14 869-878.
15 (95) Eliezer, D. In *Methods in Molecular Biology: Protein Folding Protocols*; Bai, Y.,
16 Nussinov, R., Eds.; Humana Press Inc.: Totowa, NJ, 2007; Vol. 350; pp 49-67.
17 (96) Wishart, D. S.; Bigam, C. G.; Holm, A.; Hodges, R. S.; Sykes, B. D. *J. Biomol. NMR*
18 **1995**, *5*, 67-81.
19 (97) Montaldi, L. R.; Berardi, M.; Souza, E. S.; Juliano, L.; Ito, A. S. *J. Fluoresc.* **2012**, *22*,
20 1151-1158.
21
22
23
24
25
26
27
28
29
30
31
32
33
34
35
36
37
38
39
40
41
42
43
44
45
46
47
48
49
50
51
52
53
54
55
56
57
58
59
60

1
2 For Table of Contents Only:
3
4
5

